Inelastic scattering of electrons at real metal surfaces

Z.-J. Ding

CCAST (World Laboratory), P.O. Box 8730, Beijing, 100080, People's Republic of China
and Fundamental Physics Center, University of Science and Technology of China, Hefei 230026, Anhui, People's Republic of China

A theory is presented to calculate the electron inelastic scattering cross section for a moving electron near the surface region at an arbitrary takeoff angle. The theory is based on using a bulk plasmon-pole approximation to derive the numerically computable expression of the electron self-energy in the random-phase approximation for a surface system, through the use of experimental optical constants. It is shown that the wave-vector-dependent surface dielectric function satisfies the surface sum rules in this scheme. The theory provides a detailed knowledge of electron self-energy depending on the kinetic energy, distance from surface, and velocity vector of an electron moving in any metal of a known dielectric constant, accommodating the formulation to practical situation in surface electron spectroscopies. Numerical computations of the energy-loss cross section have been made for Si and Au. The contribution to the total differential scattering cross section from each component is analyzed. The depth dependence informs us in detail how the bulk excitation mode changes to a surface excitation mode with an electron approaching the surface from the interior of a medium. [S0163-1829(97)00815-1]

I. INTRODUCTION

In the characterization of metal surfaces with electron spectroscopies, such as reflection electron energy-loss spectroscopy, Auger electron spectroscopy, and x-ray photoelectron spectroscopy, the surface electron excitation is accompanied by bulk excitation as experienced by a signal electron. The relative contribution to the total energy-loss spectrum from each channel depends strongly on an experimental configuration. It is thus important to know quantitatively how the surface excitation varies with experimental conditions and modifies the signal spectrum measured. Such a theory will be essential to extract the signal or background due to surface excitation from the overall spectrum.[1,2] Furthermore, an accurate Monte Carlo simulation of electron scattering under a surface relies critically on the scattering cross section available. Any simulation using empirical cross sections or semiempirical ones[3] loses the physical processes happening in a real case and may cause self-inconsistency.

However, the current theories of electron inelastic scattering can hardly accommodate the practical situation and provide a general description of the energy-loss processes of electrons near the surface region of materials with which we are experimentally interested. The difficulty arises from the simplification and limitation assumed by the theories.[4–18] Emphasis has been put on the surface plasmon excitation in a free-electron metal, such as Al, assuming simple electron trajectory geometry, e.g., normal or parallel movement of the charge to a surface. The present work thus aims to overcome these shortcomings within the available theoretical framework.

To simulate the response of a real metal to a charge, one may use experimental dielectric constant $\varepsilon(\omega)$ instead of the dielectric function for free-electron gas.[19] Such a useful method has been devised by Penn[20] to obtain the bulk dielectric function $\varepsilon(\mathbf{q},\omega)$ in a bulk plasmon-pole approximation.[21,22] This model dielectric function yields a quite reasonable scattering differential cross section, mean-free path, and stopping power of electrons in a bulk material.[23–27] The surface dielectric function in a surface plasmon-pole approximation[12,28] was, however, formulated to represent a surface plasmon peak solely and it is thus not suitable to describe other metals presenting a complex structure in optical energy-loss function $\text{Im}\{-1/\varepsilon(\omega)\}$. Therefore, in order to make a theory general in form and applicable to real metal surfaces, it is quite natural to derive an optical data-based surface dielectric function in the plasmon-pole approximation. To avoid a divergence problem at the surface it is necessary to consider the spatial dispersion.[12,14,17]

The best approach to the problem of interaction of a charge with a medium is given by the self-energy calculation. For a surface system, Flores and Garcia-Moliner have developed a very useful method[29] to obtain complex self-energy in quantum-mechanical formulation by using the specular surface reflection model.[30,31] An obvious advantage of the method is that it recovers other semiclassical results and provides a unified treatment. This theory forms the basis of the present study.

II. THEORY

A. General formula

We require that the metal be contained in a semi-infinite space of $z<0$. In the specular surface reflection model the induced potential is determined by the external charge, its image charge about the surface, and the fictitious surface charges fixed by the boundary conditions. Then one obtains the induced potentials for an external charge inside or outside the metal described by a dielectric function $\varepsilon(\mathbf{q},\omega)$, as[29]

$$
\Phi(zz'|\mathbf{q}_\parallel,\omega) = \begin{cases}
\dfrac{2\pi}{q_\parallel} e^{-q_\parallel(z+z')}\left\{1 - 2\varepsilon_s(\mathbf{q}_\parallel,\omega)\right\} & (z>0, z'>0); \quad (1)\\[3ex]
-\dfrac{2\pi}{q_\parallel} e^{-q_\parallel z}\left\{e^{q_\parallel z'} - 2\varepsilon_s(\mathbf{q}_\parallel,\omega)\dfrac{q_\parallel}{\pi}\int_{-\infty}^{\infty} e^{iq_\perp z'}\dfrac{dq_\perp}{q^2\varepsilon(\mathbf{q},\omega)}\right\} & (z>0, z'<0); \quad (2)\\[3ex]
-\dfrac{2\pi}{q_\parallel} e^{-q_\parallel z'}\left\{e^{q_\parallel z} - 2\varepsilon_s(\mathbf{q}_\parallel,\omega)\dfrac{q_\parallel}{\pi}\int_{-\infty}^{\infty} e^{iq_\perp z}\dfrac{dq_\perp}{q^2\varepsilon(\mathbf{q},\omega)}\right\} & (z<0, z'>0); \quad (3)\\[3ex]
\displaystyle\int_{-\infty}^{\infty} e^{iq_\perp z'} A(z|\mathbf{q},\omega)\,dq_\perp & (z<0, z'<0), \quad (4)
\end{cases}
$$

where $\mathbf{q}=(\mathbf{q}_\parallel,q_\perp)$ and

$$
A(z|\mathbf{q},\omega) = 2e^{-iq_\perp z}\left(\frac{1}{\varepsilon(\mathbf{q},\omega)} - 1\right)\frac{1}{q^2} + 2e^{iq_\perp z}\frac{1}{q^2\varepsilon(\mathbf{q},\omega)}
$$
$$
- 4\varepsilon_s(\mathbf{q}_\parallel,\omega)\frac{q_\parallel}{\pi}\frac{1}{q^2\varepsilon(\mathbf{q},\omega)}\int_{-\infty}^{\infty} e^{iq_\perp z}\frac{dq_\perp}{q^2\varepsilon(\mathbf{q},\omega)}.
$$
$$(5)$$

z and z' represent, respectively, the position of the charge and field point. Atomic units ($e=\hbar=m=1$) are used throughout. In Eq. (5) three terms explicitly display the origin of the bulk mode and the surface mode in scattering cross section, which were established by an external charge: The first term describes the screening response of infinite medium to the external charge and the second term to the image charge. Because the image charge is not realistic, there is no a bare Coulomb potential q^{-2} to be subtracted. The third one is due to the fictitious surface charges. For convenience the surface dielectric function $\varepsilon_s(\mathbf{q}_\parallel,\omega)$ in the above equations is defined, in a form differing from the others,[4,17] in terms of the bulk dielectric function by

$$
\varepsilon_s^{-1}(\mathbf{q}_\parallel,\omega) = 1 + \frac{q_\parallel}{\pi}\int_{-\infty}^{\infty}\frac{dq_\perp}{q^2\varepsilon(\mathbf{q},\omega)}. \quad (6)
$$

The self-energy operator in the random-phase approximation is given by the multiplication of the Green's function and the induced potential.[21] For a system without translational invariance in the z direction this self energy reads as

$$
\Sigma(zz'|\mathbf{q}_\parallel,\omega) = i(2\pi)^{-3}\int \Phi(zz'|\mathbf{q}_\parallel',\omega')
$$
$$
\times G_s(zz'|\mathbf{q}_\parallel-\mathbf{q}_\parallel',\omega-\omega')d\mathbf{q}_\parallel'd\omega', \quad (7)
$$

where G_s is the time-ordering surface Green's function that can be constructed from a bulk free-electron Green's function.[31] A rather considerable simplification is to consider limiting cases of surface potential U. For $U=\infty$ and $U=0$, G_s can be written explicitly and local self-energy $\Sigma(z)$ may be obtained by an integration over z'.

Flores and Garcia-Moliner have obtained the expression of $\Sigma(z)$ for an electron impacting the surface from the vacuum side, in a fast-electron approximation. Similarly, for our present purpose, we have derived the expression of $\Sigma(z)$ for an electron moving towards the surface from the interior of the medium.[32] In approaching and before arriving at the surface ($z<0, v_\perp>0$), it is given by

$$
\Sigma_{\text{in}}(z<0) = -\frac{i}{(2\pi)^3}\int d\mathbf{q}_\parallel\int_{-\infty}^{\infty} dq_\perp d\omega\, e^{iq_\perp z}\frac{A(z|\mathbf{q},\omega)}{\omega-\mathbf{q}\cdot\mathbf{v}-i\eta} = \Sigma_{\text{in}}^b + \Sigma_{\text{in}}^{b-s}(z) + \Sigma_{\text{in}}^s(z), \quad (8)
$$

for both $U=0$ and $U=\infty$. The first term, which is independent of z, is due to bulk excitation:

$$
\Sigma_{\text{in}}^b = \frac{2}{(2\pi)^2}\int\frac{d\mathbf{q}}{q^2}\int_0^{\infty} d\omega\left(\frac{1}{\varepsilon(\mathbf{q},\omega)} - 1\right)\delta(\omega-\mathbf{q}\cdot\mathbf{v}), \quad (9)
$$

where $\mathbf{v}=(\mathbf{v}_\parallel,v_\perp)$ is the electron velocity vector. All the other terms give a net surface effect. The second term, which is due to the image charge as we stated above, is the boundary correction to the bulk term due to the presence of the surface,

$$
\Sigma_{\text{in}}^{b-s}(z) = -\frac{2i}{(2\pi)^3}\int d\mathbf{q}_\parallel\int_0^{\infty} d\omega\int_{-\infty}^{\infty}\frac{dq_\perp}{q^2\varepsilon(\mathbf{q},\omega)}\left(\frac{e^{-2iq_\perp z}}{\omega-\mathbf{q}\cdot\mathbf{v}-i\eta} - \frac{e^{2iq_\perp z}}{\omega-\mathbf{q}\cdot\mathbf{v}+i\eta}\right), \quad (10)
$$

and the third term represents the surface excitation contributed by surface charges,

$$
\Sigma_{\text{in}}^s(z) = \frac{i}{2\pi^4}\int d\mathbf{q}_\parallel\int_0^{\infty} d\omega\, q_\parallel\varepsilon_s(\mathbf{q}_\parallel,\omega)\int_{-\infty}^{\infty}\frac{dq_\perp}{q^2\varepsilon(\mathbf{q},\omega)}\left(\frac{e^{-iq_\perp z}}{\omega-\mathbf{q}\cdot\mathbf{v}-i\eta} - \frac{e^{iq_\perp z}}{\omega-\mathbf{q}\cdot\mathbf{v}+i\eta}\right)\int_{-\infty}^{\infty} e^{iq_\perp z}\frac{dq_\perp}{q^2\varepsilon(\mathbf{q},\omega)}. \quad (11)
$$

When the electron is ejected into vacuum ($z>0, v_\perp>0$), we have

$$\Sigma_{\text{out}}(z>0) = -\frac{1}{2\pi^2}\int d\mathbf{q}_\parallel \frac{e^{-2q_\parallel z}}{q_\parallel}\int_0^\infty d\omega[1-2\varepsilon_s(\mathbf{q}_\parallel,\omega)]\frac{q_\parallel v_\perp}{(\omega-\mathbf{q}_\parallel\cdot\mathbf{v}_\parallel)^2+(q_\parallel v_\perp)^2}$$

$$+\frac{i}{(2\pi)^2}\int d\mathbf{q}_\parallel\frac{e^{-q_\parallel z}}{q_\parallel}\int_0^\infty d\omega\left\{\left[\frac{e^{-i(\omega-\mathbf{q}_\parallel\cdot\mathbf{v}_\parallel)z/v_\perp}}{\omega-\mathbf{q}_\parallel\cdot\mathbf{v}_\parallel-iq_\parallel v_\perp}-\text{c.c.}\right]+[1-2\varepsilon_s(\mathbf{q}_\parallel,\omega)]\left[\frac{e^{i(\omega-\mathbf{q}_\parallel\cdot\mathbf{v}_\parallel)z/v_\perp}}{\omega-\mathbf{q}_\parallel\cdot\mathbf{v}_\parallel+iq_\parallel v_\perp}-\text{c.c.}\right]\right.$$

$$\left.-2\varepsilon_s(\mathbf{q}_\parallel,\omega)\frac{q_\parallel}{\pi}\int_{-\infty}^\infty\frac{dq_\perp}{q^2\varepsilon(\mathbf{q},\omega)}\left[\frac{e^{-i(\omega-\mathbf{q}_\parallel\cdot\mathbf{v}_\parallel)z/v_\perp}}{\omega-\mathbf{q}\cdot\mathbf{v}-i\eta}-\text{c.c.}\right]\right\}, \tag{12}$$

for $U=0$. Of course, for $U=\infty$, we would not have the electron trajectory penetrating the surface and the theory yields instead $\Sigma_{\text{out}}(z<0)$ for a reflected electron trajectory leaving the surface.

The first integral term in Eq. (12) is the same as the self-energy for an electron incident into the surface from the vacuum side, $\Sigma_{\text{in}}(z>0)$, and also agrees with a semiclassical result. The second term has a known oscillatory behavior in z,[12] indicating a wake surface excitation trailing the particle by the wake potential. The phenomenon is similar to that on the bulk side when a particle penetrates into the metal from a vacuum;[23] however, its intensity is weaker because it lacks dense free electrons in the vacuum side. For a parallel electron trajectory to the surface, $v_\perp=0$, this term vanishes and we cannot expect an oscillatory scattering cross section.

The continuity of Eqs. (8) and (12) at $z=0$ holds,

$$\Sigma_{\text{in}}(0^-)=\Sigma_{\text{out}}(0^+)=-\frac{1}{2\pi^2}\int\frac{d\mathbf{q}}{q^2}\int_0^\infty d\omega\,\delta(\omega-\mathbf{q}\cdot\mathbf{v})+\frac{1}{\pi^2}\int d\mathbf{q}_\parallel\int_0^\infty d\omega\,\varepsilon_s(\mathbf{q}_\parallel,\omega)\int_{-\infty}^\infty\frac{dq_\perp}{q^2\varepsilon(\mathbf{q},\omega)}\delta(\omega-\mathbf{q}\cdot\mathbf{v}). \tag{13}$$

In the following discussion, we shall concentrate only on the imaginary part of Eq. (8). But the formulation presented in the following section can also be applied to other theories dealing with surface problems.

B. Plasmon-pole approximation

The dielectric function for a single plasmon of energy ω_p may be approximated as

$$\varepsilon(q,\omega;\omega_p)=1+\frac{\omega_p^2}{\omega_q^2-\omega_p^2-\omega(\omega+i\gamma_q)}, \tag{14}$$

where ω_q satisfies a dispersion relation $\omega_q=\omega_q(q,\omega_p)$ and equals ω_p at $q=0$. For the infinitesimal damping constant γ_q we then have

$$\lim_{\gamma_q\to0^+}\text{Re}\left\{\frac{1}{\varepsilon(q,\omega;\omega_p)}-1\right\}=\mathcal{P}\frac{\omega_p^2}{\omega^2-\omega_p^2} \tag{15}$$

$$\lim_{\gamma_q\to0^+}\text{Im}\left\{\frac{-1}{\varepsilon(q,\omega;\omega_p)}\right\}=\pi\omega_p^2\delta(\omega^2-\omega_q^2)$$

$$=\frac{\pi}{2}\frac{\omega_p^2}{\omega_q}\delta(\omega-\omega_q)$$

$$(\omega>0), \tag{16}$$

where $\mathcal{P}$ denotes Cauchy principal value.

In the spirit of a statistical approach,[34] Penn has proposed a general model of dielectric function. The extended energy-loss function is written as

$$\text{Im}\left\{\frac{-1}{\varepsilon(q,\omega)}\right\}=\int_0^\infty d\omega_p G(\omega_p)\text{Im}\left\{\frac{-1}{\varepsilon(q,\omega;\omega_p)}\right\}, \tag{17}$$

where the expansion coefficient $G(\omega)$ relates to optical energy-loss function by

$$G(\omega)=\frac{2}{\pi\omega}\text{Im}\left\{\frac{-1}{\varepsilon(\omega)}\right\}. \tag{18}$$

Using Kramers-Kronig relation it is trivial to obtain the corresponding relation for the real part of the inverse of dielectric function,

$$\text{Re}\left\{\frac{1}{\varepsilon(q,\omega)}-1\right\}=\int_0^\infty d\omega_p G(\omega_p)\text{Re}\left\{\frac{1}{\varepsilon(q,\omega;\omega_p)}-1\right\}. \tag{19}$$

Equations (17) and (19) may be combined to a single equation written as

$$\frac{1}{\varepsilon(q,\omega)}-1=\int_0^\infty d\omega_p G(\omega_p)\left[\frac{1}{\varepsilon(q,\omega;\omega_p)}-1\right]$$

$$=\int_0^\infty d\omega_p H(\omega_p)\left[\frac{1}{\omega_q+\omega+i\eta}-\frac{1}{\omega_q-\omega-i\eta}\right], \tag{20}$$

where η is an infinitesimal quantity and

$$H(\omega_p) = \frac{\omega_p^2}{2\omega} G(\omega_p) = \frac{1}{\pi} \frac{\omega_p}{\omega} \text{Im}\left\{\frac{-1}{\varepsilon(\omega_p)}\right\} \qquad (21)$$

is real for $\omega > 0$.

Using of Eq. (20) in Eq. (8) one can obtain the values of complex self-energy for a metal of known dielectric con-

stant. To be more explicit, we consider a simple dispersion relation[19,26]

$$\omega_q = \omega_p + \tfrac{1}{2} q^2, \qquad (22)$$

with which the integration over $q_\perp$ can be analytically given. By substituting Eq. (A1) into Eq. (6) we derive the expression of $\varepsilon_s^{-1}(q_\parallel, \omega)$ given by

$$\text{Re}\left\{\frac{1}{\varepsilon_s(q_\parallel, \omega)} - 1\right\} = \text{Re}\left\{\frac{1}{\varepsilon(\omega)}\right\} - \frac{1}{\pi\omega} \int_0^\infty d\omega_p \text{Im}\left\{\frac{-1}{\varepsilon(\omega_p)}\right\}$$

$$\times \left[\frac{\omega_p}{(\omega+\omega_p)\sqrt{2(\omega+\omega_p)/q_\parallel^2+1}} + \mathcal{P}\frac{\omega_p \theta(\omega_p - \omega + q_\parallel^2/2)}{(\omega-\omega_p)\sqrt{2(\omega_p-\omega)/q_\parallel^2+1}}\right] \qquad (23)$$

and

$$\text{Im}\left\{\frac{-1}{\varepsilon_s(q_\parallel, \omega)}\right\} = \frac{1}{\pi\omega} \int_0^\infty d\omega_p \text{Im}\left\{\frac{-1}{\varepsilon(\omega_p)}\right\} \frac{\omega_p \theta(\omega - \omega_p - q_\parallel^2/2)}{(\omega-\omega_p)\sqrt{2(\omega-\omega_p)/q_\parallel^2-1}}, \qquad (24)$$

where $\theta(x)$ is the step function ($=1$ if $x>0$; 0 otherwise). Making use of the Kramers-Kronig relation, the first term in Eq. (A1) yields the first term in Eq. (23).

Finally we find the expression for imaginary part of the self-energy term written as (see Appendix A)

$$\text{Im}\Sigma_{\text{in}}^{b\text{-}s}(z) = -\frac{1}{(2\pi)^2} \int d\mathbf{q}_\parallel \int_0^\infty \frac{d\omega}{\omega} \int_0^\infty d\omega_p \omega_p \text{Im}\left\{\frac{-1}{\varepsilon(\omega_p)}\right\} \frac{\theta(\omega - \omega_p - q_\parallel^2/2)}{(\omega-\omega_p)\sqrt{2(\omega-\omega_p)-q_\parallel^2}} \left[\delta(\omega - \mathbf{q}_\parallel \cdot \mathbf{v}_\parallel - \sqrt{2(\omega-\omega_p)-q_\parallel^2}v_\perp)\right.$$

$$\left. + \delta(\omega - \mathbf{q}_\parallel \cdot \mathbf{v}_\parallel + \sqrt{2(\omega-\omega_p)-q_\parallel^2}v_\perp)\right]\cos[2\sqrt{2(\omega-\omega_p)-q_\parallel^2}z]. \qquad (25)$$

The imaginary part of $\Sigma_{\text{in}}^s(z)$ can also be written, though tediously, with Eqs. (23), (24), (A2), (A7), and (A8).

Performing further angular integration (see Appendix B) we can obtain the double differential cross section in wave vector and frequency for electron inelastic scattering near the surface, $p(z|q_\parallel, \omega)$, defined by

$$-2\,\text{Im}\,\Sigma(z) = v \int_0^\infty dq_\parallel \int_0^\infty d\omega\, p(z|q_\parallel, \omega), \qquad (26)$$

and the differential cross section in frequency:

$$p(z|\omega) = \int_0^\infty dq_\parallel p(z|q_\parallel, \omega), \qquad (27)$$

where the dependence on the kinetic energy and moving direction is implied. For the bulk scattering term it is simply given by[25]

$$p^b(\omega) = \frac{1}{\pi v^2 \omega} \int_0^\infty d\omega_p \frac{\omega_p}{\omega - \omega_p} \text{Im}\left\{\frac{-1}{\varepsilon(\omega_p)}\right\}$$

$$\times \theta(v\bar{q} - \tfrac{1}{2}\bar{q}^2 - \omega), \qquad (28)$$

where $\omega = \omega_q(\bar{q}, \omega_p)$ and the step function represents energy and momentum conservation. This equation involves a single integration, while for surface scattering terms we have to perform numerical multiple integration.

C. Numerical method

For calculation of double differential cross section we must perform numerical integration involving the optical-dielectric constant $\varepsilon(\omega_p)$ over the photon energy ω_p. Differing from Eq. (28), the integration should be carried out over the entire energy range from 10^{-1} eV up to the energy region of inner-shell electrons. Some terms, such as the first terms in Eqs. (23) and (A2), may avoid doing so by direct use of $\text{Re}\{1/\varepsilon(\omega_p)\}$. We empirically found that the integration requires very thin grid spacing in order to get a reasonably smooth curve. It may mainly be due to the difficulty of convergence problems for the Cauchy principal integral. Though some numerical techniques[35] may be modified to speed up the computation, we have used the conventional numerical integration procedure incorporating some analytical expressions.

We first divide the whole energy range by a grid of fixed numbers with unequal steps. The width of the steps begins with 10^{-3} eV from $\omega_p = 0.1$ eV and is 0.01 eV for $1 < \omega_p < 100$ eV. It increases by order with $\omega_p > 100$ eV. In between two grid points the Romberg integration routine is applied. It may be noted that the variation of the optical energy-loss function $\text{Im}\{-1/\varepsilon(\omega_p)\}$ with ω_p is not dramatic. In the energy region 10–10^2 eV, the most steep change occurs within the zone $\Delta\omega_p \sim 0.1$ eV (e.g., for Ag), and ~ 1 eV at an inner-shell edge in region $\omega_p \sim 1$ keV. Hence, for a grid spacing chosen much less than $\Delta\omega_p$ we can regard $\text{Im}\{-1/\varepsilon(\omega_p)\}$ linear in the grid interval and derive an analytical expression for this integration section. This enables the calculation to be made faster and maintains accuracy. It

also avoids the divergence problem in evaluating the Cauchy principal integral. Furthermore, the analytical formula may be used to show that Eq. (30) is valid in every small interval and, hence, in the whole energy range. However, the analytical expression can only be given for integrals in Eqs. (23) and (24); other integrals still require Romberg integration. For the angular integration of Eq. (25) we may use Eq. (B3) to shorten the integration steps.

When the values of $p(z|q_\parallel,\omega)$ are calculated, a similar Romberg procedure is used to find $p(z|\omega)$ in Eq. (27). The range of $q_\parallel$ from 0 to 1 $\mathring{A}^{-1}$ is divided by a mesh of 40 points. The convergence is tested to an absolute error of 10^{-4} $(\text{keV } \mathring{A})^{-1}$. When an electron moves nearly parallel to the surface, the finer $q_\parallel$ segment is necessary. This will be understood from the plot of double differential cross sections shown later.

III. RESULTS AND DISCUSSION

A. Surface energy-loss function and sum rules

We consider now Si and Au as examples of application of the present theory. Si presents a typical nearly-free-electron-like behavior in bulk energy-loss function by showing a bulk plasmon peak of finite width. Au demonstrates a complex structure in energy-loss function due to interband transitions, which is common to most real metals.

Figure 1 shows the surface energy-loss function $\text{Im}\{\varepsilon_s(q_\parallel,\omega)\}$ for several representative values of $q_\parallel$ and the comparison with the optical bulk energy-loss function $\text{Im}\{-1/\varepsilon(\omega)\}$ and with the optical surface energy-loss function $\text{Im}\{-1/[1+\varepsilon(\omega)]\}$. It can be seen that $\text{Im}\{\varepsilon_s(q_\parallel,\omega)\}$ agrees with the optical surface energy-loss function at $q_\parallel=0$. This may be understood if we replace the nonlocal dielectric function $\varepsilon(q,\omega)$ by the local one $\varepsilon(\omega)$ in the definition equation of the surface dielectric function, Eq. (6). The exact verification can be done if we take the limit

$$\lim_{q_\parallel \to 0} \frac{\theta(\omega-\omega_p-q_\parallel^2/2)}{(\omega-\omega_p)\sqrt{2(\omega-\omega_p)/q_\parallel^2-1}} = \pi\delta(\omega-\omega_p) \quad (29)$$

in Eq. (24). Taking also the limit in Eq. (23), the integral terms vanish. Hence, we have

$$\varepsilon_s^{-1}(0,\omega) = 1 + \varepsilon^{-1}(\omega). \quad (30)$$

so that $\text{Im}\{\varepsilon_s(0,\omega)\}=\text{Im}\{-1/[1+\varepsilon(\omega)]\}$.

Figure 2 demonstrates the perspective plot of the surface energy-loss function that resembles in appearance the bulk energy-loss function, $\text{Im}\{-1/\varepsilon(q,\omega)\}$, obtained in the plasmon-pole approximation (Fig. 1 in Ref. 25). The surface plasmon energy starts from $1/\sqrt{2}$ of the bulk plasmon energy at $q_\parallel=0$ and increases with $q_\parallel$ nearly in a parabolic curve. To see this we put in Eqs. (23) and (24) the single plasmon-pole terms,
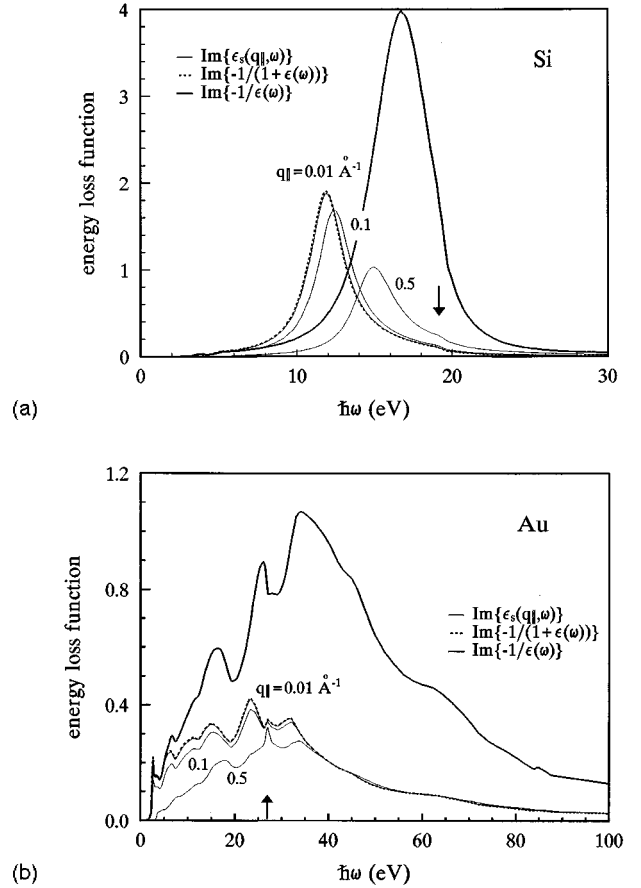

FIG. 1. Plots of the energy-loss functions calculated from optical data. Thin solid lines represent surface energy-loss function $\text{Im}\{\varepsilon_s(q_\parallel,\omega)\}$ for several representative values of $q_\parallel$. Arrow indicates ghost peak caused by discontinuity of optical constants. The dashed line and solid line are, respectively, the optical surface energy-loss function $\text{Im}\{-1/(1+\varepsilon(\omega))\}$ and optical bulk energy-loss function $\text{Im}\{-1/\varepsilon(\omega)\}$. (a) Si and (b) Au.

$$\text{Re}\left\{\frac{1}{\varepsilon(\omega)}\right\} = 1 + \mathcal{P}\frac{\omega_b^2}{\omega^2-\omega_b^2},$$

$$\text{Im}\left\{\frac{-1}{\varepsilon(\omega)}\right\} = \frac{\pi}{2}\omega_b\delta(\omega-\omega_b), \quad (31)$$

where ω_b is the bulk plasmon energy. The dispersion of surface plasmon is found from $\text{Re}\{1/\varepsilon_s(q_\parallel,\omega_s)\}=0$ or

$$2x(2x^2-1) = \frac{x-1}{\sqrt{1+2(1+x)\omega_b/q_\parallel^2}} + \frac{1+x}{\sqrt{1+2(1-x)\omega_b/q_\parallel^2}}, \quad (32)$$

where $x=\omega_s/\omega_b$ and ω_s is the surface plasmon energy. Obviously, $\omega_s=\omega_b/\sqrt{2}$ at $q_\parallel=0$. The dispersion curve fitted to a quadratic is similar to that shown in Fig. 1 of Ref. 30, having a positive coefficient in linear $q_\parallel$. Though experimental measurements show that the surface plasmon dispersion is negative at small $q_\parallel$,[36,37] the present simple theory does not allow us to describe such a negative dispersion as shown by density-function theories.[38,39] However, a slight negative dispersion should not have a strong effect on the values of scattering cross sections.
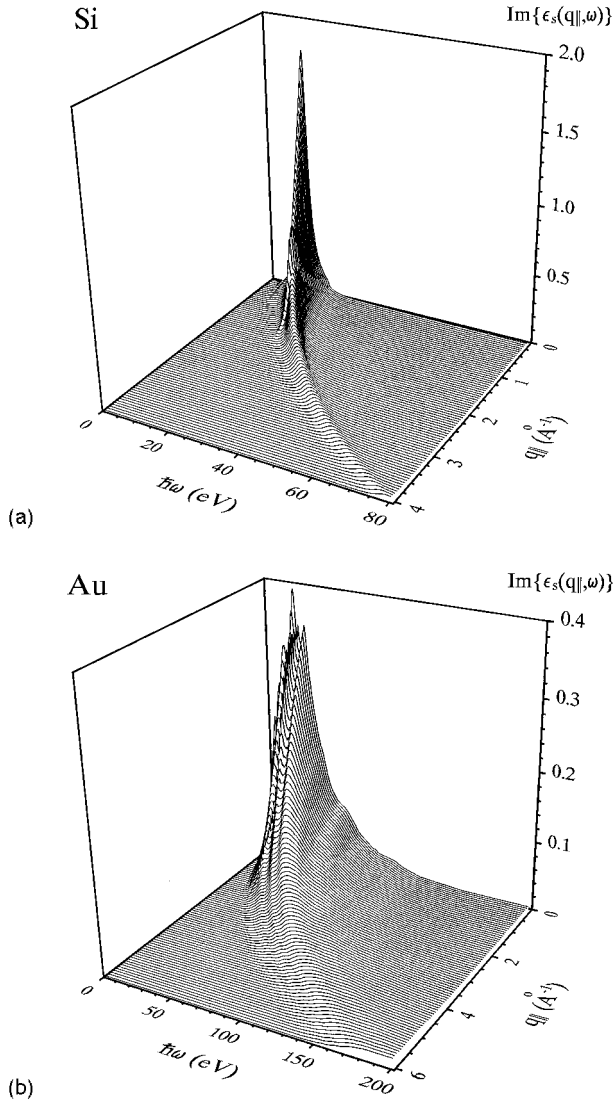
Si

$\mathrm{Im}\{\epsilon_s(q_\parallel,\omega)\}$

(a)

Au

$\mathrm{Im}\{\epsilon_s(q_\parallel,\omega)\}$

(b)

FIG. 2. Perspective view of the energy-loss ω-dependent and horizontal momentum transfer $q_\parallel$-dependent surface energy-loss function. (a) Si and (b) Au.

In Figs. 1 and 2 some ghost peak or shoulder are seen in surface energy-loss function. The peak position does not change with $q_\parallel$. We found that it is caused by the discontinuity of optical constants[40] that are compiled from the measurements done by different investigators. The discontinuity can hardly be observed in bulk energy-loss function but it is sensitive to the wave-vector-dependent surface energy-loss function. To remove the peak a Kramers-Kronig analysis of optical data should be done. However, in this calculation we have not attempted to do so and raw data are used directly.

Now let us consider the sum rules satisfied by the surface energy-loss function. From Eqs. (16)–(18) it is trivial to verify that the perfect screening sum rule[41]

$$\mu_{-1}^b = \lim_{q \to 0} \int_0^\infty \frac{1}{\omega} \mathrm{Im}\left\{ \frac{-1}{\varepsilon(q,\omega)} \right\} d\omega = \frac{\pi}{2} \qquad (33)$$

and f-sum rule

$$\mu_1^b(q) = \int_0^\infty \omega\, \mathrm{Im}\left\{ \frac{-1}{\varepsilon(q,\omega)} \right\} d\omega = \frac{\pi}{2}\, \Omega_b^2, \qquad (34)$$

where $\Omega_b = \sqrt{4\pi N e^2/m}$, are valid for plasmon-pole approximated bulk energy-loss function. Correspondingly, one can prove the sum rule

$$\mu_{-1}^s = \lim_{q_\parallel \to 0} \int_0^\infty \frac{1}{\omega} \mathrm{Im}\left\{ \frac{-1}{\varepsilon_s(q_\parallel,\omega)} \right\} d\omega = \frac{\pi}{2} \qquad (35)$$

by using the equation

$$\frac{q_\parallel}{\pi} \int_{-\infty}^\infty \frac{dq_\perp}{q^2 \omega_q^2} = \frac{q_\parallel}{\pi} \int_{-\infty}^\infty \frac{dq_\perp}{(q_\parallel^2 + q_\perp^2)[\omega_p + \frac{1}{2}(q_\parallel^2 + q_\perp^2)]}$$

$$= \frac{1}{\omega_p^2} \left[1 - \frac{q_\parallel}{\sqrt{q_\parallel^2 + 2\omega_p}} - \frac{q_\parallel \omega_p}{q_\parallel^2 + 2\omega_p} \right]. \qquad (36)$$

It is also easy to verify directly from Eq. (33) the equation

$$\mu_1^s(q_\parallel) = \int_0^\infty \omega\, \mathrm{Im}\left\{ \frac{-1}{\varepsilon_s(q_\parallel,\omega)} \right\} d\omega = \frac{\pi}{2}\, \Omega_b^2. \qquad (37)$$

However, what we are interested in here is the sum rules applied to surface energy-loss function $\mathrm{Im}\{\varepsilon_s(q_\parallel,\omega)\}$. Defining the surface response function[28] $R(\mathbf{q}_\parallel,\omega)$ and spectral function[42] $S(\mathbf{q}_\parallel,\omega)$ as

$$R(\mathbf{q}_\parallel,\omega) = 1 - 2\varepsilon_s(\mathbf{q}_\parallel,\omega) = \int_0^\infty d\omega'\, S(\mathbf{q}_\parallel,\omega')$$

$$\times \left[\frac{1}{\omega - \omega' + i\eta} - \frac{1}{\omega + \omega' + i\eta} \right], \qquad (38)$$

the imaginary part of the above equation is

$$S(\mathbf{q}_\parallel,\omega) = -\frac{1}{\pi} \mathrm{Im}\{R(\mathbf{q}_\parallel,\omega)\} = \frac{2}{\pi} \mathrm{Im}\{\varepsilon_s(\mathbf{q}_\parallel,\omega)\} \quad (39)$$

and the real part is hence just the Kramers-Kronig relation for the surface response function. It is interesting to note that the formal identity

$$\frac{1}{\varepsilon(q,\omega)} - 1 = -\frac{1}{\pi} \int_0^\infty d\omega'\, \mathrm{Im}\left\{ \frac{1}{\varepsilon(q,\omega')} - 1 \right\}$$

$$\times \left[\frac{1}{\omega - \omega' + i\eta} - \frac{1}{\omega + \omega' + i\eta} \right] \qquad (40)$$

is the counterpart of Eq. (38) for the bulk response function. When Eq. (17) is substituted into the above equation we certainly derive Eq. (20).

From the sum rules[42,43] required for $S(\mathbf{q}_\parallel,\omega)$ we should have the surface perfect-screening sum rule

$$\nu_{-1}^s = \lim_{q_\parallel \to 0} \int_0^\infty \frac{1}{\omega} \mathrm{Im}\{\varepsilon_s(q_\parallel,\omega)\} d\omega = \frac{\pi}{4} \qquad (41)$$

and the surface f-sum rule

TABLE I. Comparison of the theoretical surface perfect screening sum rules, μ^s_{-1} and ν^s_{-1}, and surface f-sum rules, $\mu^s_1(q_\parallel)$ and $\nu^s_1(q_\parallel)$, with the computed values.

	μ^s_{-1}			ν^s_{-1}			μ^s_{-1}/ν^s_{-1}		
	Theory	Calc.	Error (%)	Theory	Calc.	Error (%)	Theory	Calc.	Error (%)
Si	1.5708	1.3782	−12.26	0.7854	0.6585	−16.15	2	2.093	4.64
Au	1.5708	1.7125	9.02	0.7854	0.8265	5.23	2	2.072	3.61

	$\mu^s_1(q_\parallel)$ (eV^2)			$\nu^s_1(q_\parallel)$ (eV^2)			$\mu^s_1(q_\parallel)/\nu^s_1(q_\parallel)$		
$q_\parallel$ (Å^{-1})	Theory	Calc.	Error (%)	Theory	Calc.	Error (%)	Theory	Calc.	Error (%)
0.0	1 514.9	1418.1	−6.39	378.73	359.45	−5.09	4	3.95	−1.37
0.5	1 514.9	1399.3	−7.63	378.73	355.55	−6.12	4	3.94	−1.61
1.0	1 514.9	1380.0	−8.90	378.73	350.74	−7.39	4	3.93	−1.63
0.0	10 086.2	9203.6	−8.75	2521.6	2283.0	−9.46	4	4.03	0.78
0.5	10 086.2	9153.8	−9.24	2521.6	2274.9	−9.78	4	4.02	0.60
1.0	10 086.2	9097.2	−9.80	2521.6	2262.1	−10.29	4	4.02	0.54

$$\nu^s_1(q_\parallel) = \int_0^\infty \omega \, \text{Im}\{\varepsilon_s(q_\parallel, \omega)\} d\omega = \frac{\pi}{4} \Omega^2_s, \qquad (42)$$

where $\Omega_s = \Omega_b/\sqrt{2}$.

Because the present theory gives the analytical expression only for the inverse of the surface dielectric function, the surface energy-loss function cannot be written in a simple expression. Therefore, Eqs. (41) and (42) are hardly to be proved analytically and a numerical verification is necessary. It has been shown[44] that they are valid at $q_\parallel = 0$ for optical surface energy-loss function. For arbitrary $q_\parallel$ values, we may take the ratio

$$\frac{\mu^s_1(q_\parallel)}{\nu^s_1(q_\parallel)} = 4, \quad \frac{\mu^s_{-1}}{\nu^s_{-1}} = 2. \qquad (43)$$

Table I verifies the tests of the surface perfect screening sum rule and the surface f-sum rule. The absolute value of the calculation deviates slightly from theoretical value to the same extent as for the bulk sum rules.[24] This is reasonable considering the uncertainties involved in the experimental data of the dielectric constant. However, the uncertainty may be largely canceled out by taking the ratio so that Eq. (43) is satisfied quite well for the present wave-vector-dependent surface energy-loss function.

B. Double differential cross section

The total cross section differential in $q_\parallel$ and ω has two components, i.e., $p^{b-s}(z|q_\parallel, \omega)$ and $p^s(z|q_\parallel, \omega)$. The bulk term $p^b(q, \omega)$ is essentially differential in q and ω and we have not tried to integrate it over the $q_\perp$ component. Figure 3 shows the cross section for a small value of $q_\parallel$. One can see that the image charge contributes to an increase of the scattering cross section at bulk plasmon energy in the case shown; the surface charges set up an energy-loss mechanism by surface plasmon excitation and reduce the probability of bulk plasmon excitation. The net surface effect, $p^{b-s} + p^s$, has a peak at the surface plasmon energy and a valley at the bulk plasmon energy. For large $-z$ values, both the height of the peak and valley would be smaller so that the bulk excitation mechanism dominates the overall scattering probability.

Figures 4 and 5 illustrate, respectively, the perspective view of double differential cross sections, p^{b-s} and p^s, for different values of takeoff angle ϑ defined as the angle between velocity vector and surface normal. The position of
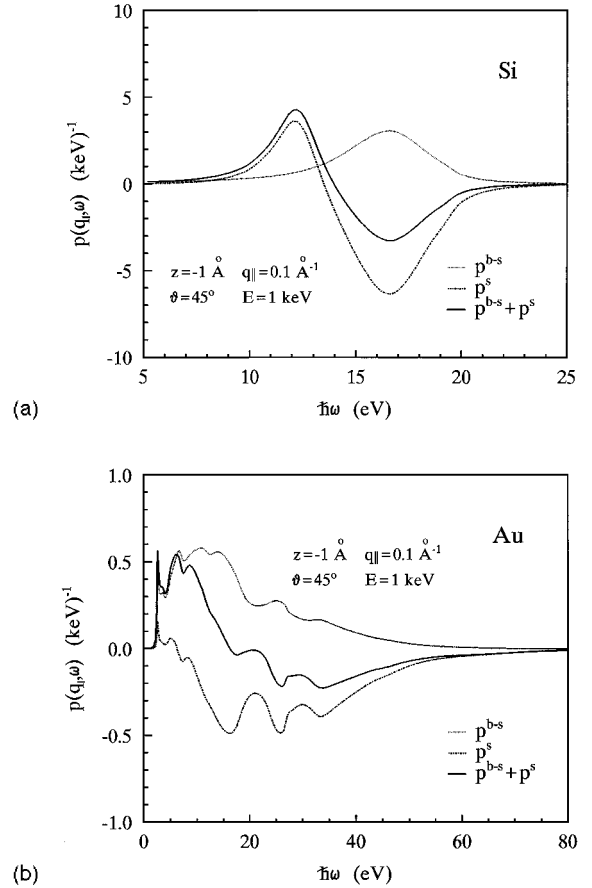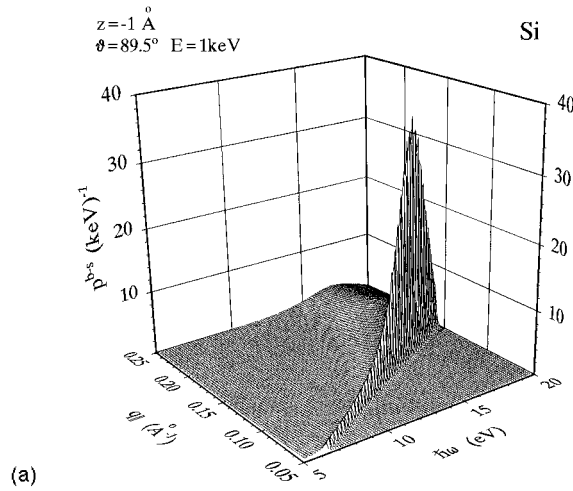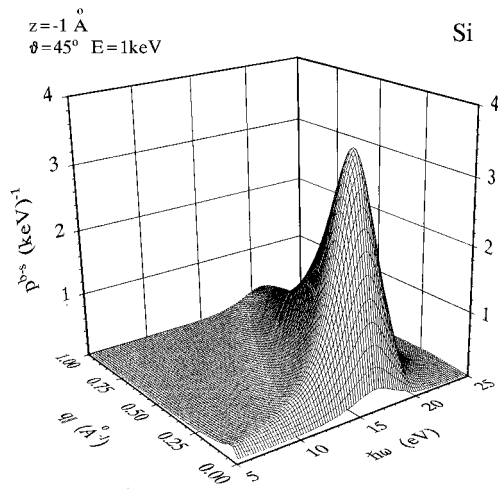

(a)

(b)

FIG. 3. Plots of the double differential cross section as a function of ω at a given value of the horizontal wave vector $q_\parallel$, depth z, takeoff angle ϑ, and kinetic energy E. The dotted and dashed lines represent, respectively, the component $p^{b-s}(q_\parallel, \omega)$ due to image charge and $p^s(q_\parallel, \omega)$ to surface charges. The solid line is their sum. (a) Si and (b) Au.

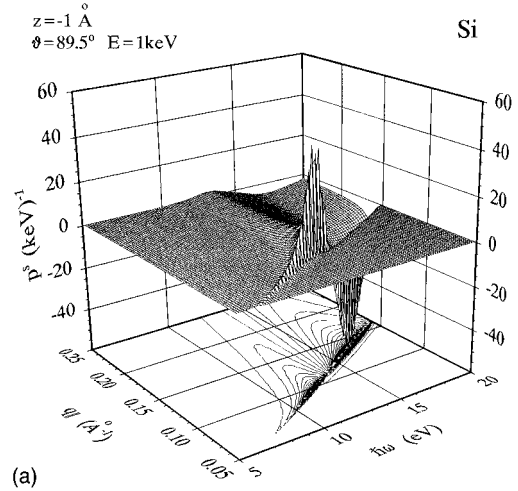FIG. 4. Perspective view of the energy-loss ω-dependent and horizontal momentum transfer $q_\parallel$-dependent double differential cross-section term $p^{b-s}(q_\parallel,\omega)$ due to image charge for takeoff angles (a) 89.5° and (b) 45°. Note that the scales are different.
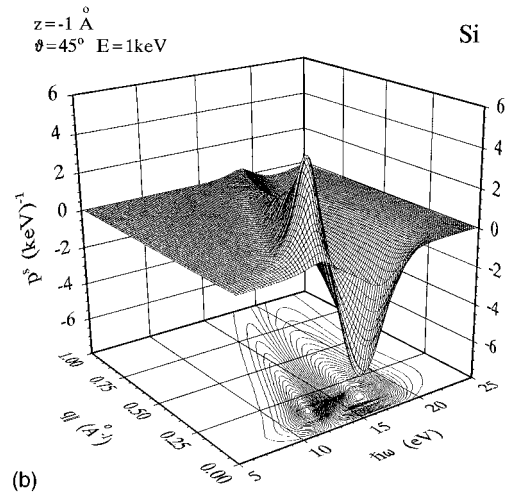

FIG. 5. Perspective view of the energy-loss ω-dependent and horizontal momentum transfer $q_\parallel$-dependent double differential cross-section term $p^{s}(q_\parallel,\omega)$ due to surface charges for takeoff angles (a) 89.5° and (b) 45°. Note that the scales are different.

both the surface plasmon peak and bulk plasmon valley shifts to the higher-energy side with the increasing of $q_\parallel$ due to dispersion. The surface dispersion starts from the surface plasmon energy and bulk dispersion from the bulk plasmon energy as shown by Figs. 4(b) and 5(b). The Bethe ridge may be more clearly seen from the bulk scattering term, $p^b(q,\omega)\propto \text{Im}\{-1/\varepsilon(q,\omega)\}$.

It is interesting to note that, in the case of glancing ejection, the ridge of p^{b-s} and p^s shrinks to a sharp plane. At small values of $q_\parallel$ there is only a δ-function-like surface plasmon peak in $p^s(q_\parallel,\omega)$ and a bulk plasmon peak in $p^{b-s}(q_\parallel,\omega)$. For large $q_\parallel$'s both these peaks reduce to a broadened hump and a negative δ-function-like bulk plasmon peak appears in $p^s(q_\parallel,\omega)$.

However, in Figs. 4(a) and 5(a) the δ-like peaks do not converge to the surface plasmon and bulk plasmon energies as $q_\parallel$ approaches zero. This is because in Eq. (25), in addition to the restriction due to the dispersion relation $\omega \geqslant \omega_p + q_\parallel^2/2$, there is a $\delta(\omega - \mathbf{q}_\parallel \cdot \mathbf{v}_\parallel)$ term imposed on the excitation probability at grazing condition, $v_\perp \approx 0$. Its angular integration, Eq. (B1), then restricts $q_\parallel \geqslant \omega/v$. Furthermore, similar to Eq. (29), it becomes a δ-function requiring $q_\parallel = \omega/v$ for $v_\perp \rightarrow 0$.

Physically, this means the resonant interaction of electrons with plasmon waves whose phase velocity is $\omega/q_\parallel$, when an electron can spend a long time in its movement parallel to the surface.[45,46] In Fig. 4(a) the bulk plasmon peak at the sharp plane is thus located at the intersection of dispersion with the resonant condition in the $(q_\parallel,\omega)$ plane. Therefore, in the case shown by Figs. 4(a) and 5(a), the surface charges enables the resonant surface plasmon excitation and the resonant bulk plasmon deexcitation, and the image charge makes the resonant bulk plasmon excitation.

C. Differential cross section

In Fig. 6 the contributions to the total differential cross section in energy from each component, bulk term $p^b(\omega)$, image charge term $p^{b-s}(z|\omega)$, and surface charge term $p^s(z|\omega)$, are shown. For Si, we found again that the net surface effect $p^{b-s}+p^s$ builds a surface plasmon mode and diminishes a bulk plasmon mode. However, for $z \sim 0$, there still remain some probabilities of energy loss around the bulk plasmon energy. Part of this can be attributed to the surface plasmon dispersion. Furthermore, the bulk plasmon excita-
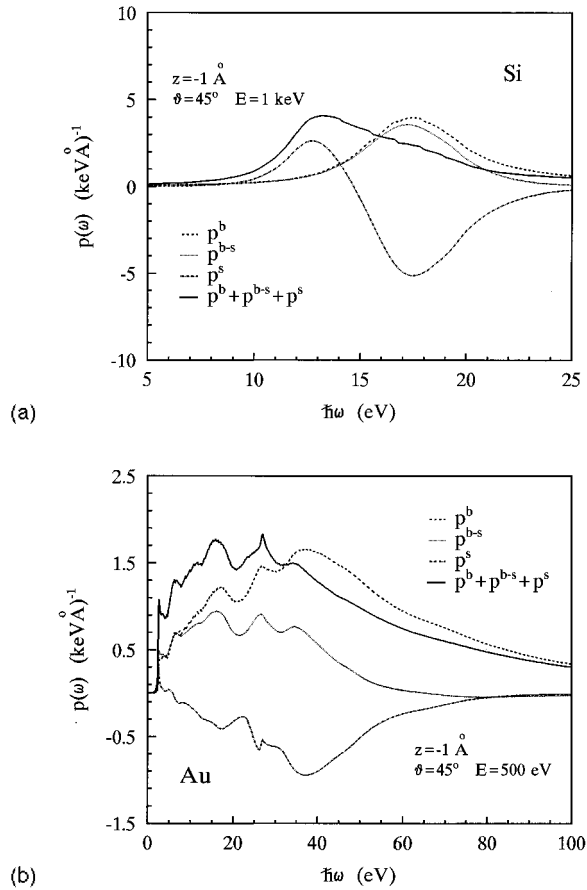
(a)

(b)

FIG. 6. Plots of the differential cross section as a function of ω at a given value of depth z, takeoff angle ϑ, and kinetic energy E. The dashed, dotted, and chain lines represent, respectively, the bulk term $p^b(\omega)$, image charge term $p^{b-s}(\omega)$, and surface charge term $p^s(\omega)$. The solid line is their sum, which is the total differential cross section. (a) Si and (b) Au.

tion peak and hence, the surface plasmon excitation peak have a large width so that the tail of the surface plasmon peak enters the energy region of the bulk plasmon peak.

An interesting case is Au. It is hard to identify the unique characteristic energy for the bulk mode and surface mode. Both modes have displayed a broadened distribution. The difference is mainly that the distribution of the surface mode has a stronger intensity in a low-energy region when compared with that of the bulk mode. The surface charge term has a contrary variation of intensity to the image charge term and bulk term. But, there is an exception for the sharp peak at 2.6 eV that is clearly presented as a surface effect. Though the peak is also observable in the bulk energy-loss function it is only shown as a shoulder in $p^b(\omega)$. Hence, the peak at 2.6 eV may be largely associated with a surface mode. The same conclusion has been made from a discussion of the optical energy-loss function,[47] although a band-structure calculation has indicated that it may also be assigned to an interband transition.[48] The present theory is successful in providing a more intimate insight into this seemingly controversial surface mode: The surface plasmon whose energy is modified by an interband transition has a dominant contribution in excitation from the surface effect. The energy-loss peak has

been experimentally observed by electron energy-loss spectroscopy both in the transmission mode[47,49] and in the reflection mode.[50,51] Figure 8 of Ref. 51 provides a detailed loss structure with a good energy resolution; all the loss peaks correspond well in position with those shown by $p(z|\omega)$ in Fig. 6(b) except that a ghost peak at 27 eV in Fig. 6(b) is caused by the discontinuity of optical data, as mentioned above. For small $-z$ and large ϑ the overall shape of $p(z|\omega)$ is quite similar to that of the optical surface energy-loss function shown in Fig. 1.

We may now compare qualitatively the result with other models that were used to obtain energy-loss cross section from experimental energy-loss spectra. It can be seen from Fig. 13 of Ref. 2 that a total trajectory energy-loss model yields two broad peaks at 3 and 5 eV. Figure 7 of Ref. 3, which shows an energy-loss function compromising surface and bulk effects, presents strong peaks at 7, 14, and 24 eV. Both their experimental cross sections display strong intensities at lower energies. Because of the approximation used and limitation inherent in extracting experimental cross-section data from experimental loss spectra, a lot of information is lost. Furthermore, some fine structures cannot be observed. A feature of these models[2,3,52] for reflection electron energy-loss spectroscopy is that they give an energy-loss probability effectively integrated over the depth z.

An improvement calculation[53] to Ref. 3 shows a compromising energy-loss function being close to the surface energy-loss function in shape. Hence, the differential cross section obtained with this energy-loss function would be closer to the present calculation if the depth dependence could be ignored. In Fig. 4 of Ref. 45 the peaks at 3.1, 5.6, and 16.1 eV correspond to those at 2.6, 6.2, and 15.8 eV in Fig. 6. It can also be seen from Fig. 5 of Ref. 45 that their experimental compromising energy-loss function is larger than the bulk energy-loss function and the surface energy-loss function by about three times. With the present theory this can be understood qualitatively. One may note that the present total differential cross section $p(z|\omega)$ is comparable in intensity to the bulk scattering cross section $p^b(\omega)$. Also, one should consider the fact that outside the metal, electrons can still excite the surface mode according to Eq. (12). For a reflection electron energy-loss spectra the surface contribution is enhanced because a backscattering electron penetrates a surface twice, and there is a net energy loss along the trajectory outside the metal.[29]

Figures 7 and 8 show the z dependence of the total differential cross section for several values of ϑ. For Si, the transition from bulk plasmon excitation to surface plasmon excitation as an electron approaches the surface from the deep interior of the medium can be clearly seen. At a glancing condition $\vartheta=89.5°$, the most probable excitation of the surface plasmon is not on the geometrical surface ($z=0$), but at some distance underneath. This result should agree quantitatively with that obtained by Zabala and Echenique[17] because it has been shown[32] that the present theory reproduces their cross section for parallel electron trajectory. The result also agrees qualitatively with other recent calculations[54,55] in which the average over the electron trajectory has been taken. For Au, it is interesting to see how each peak in $p(z|\omega)$ varies with z. The intensity for some peaks changes quickly while others change slowly. Again, the most prob-
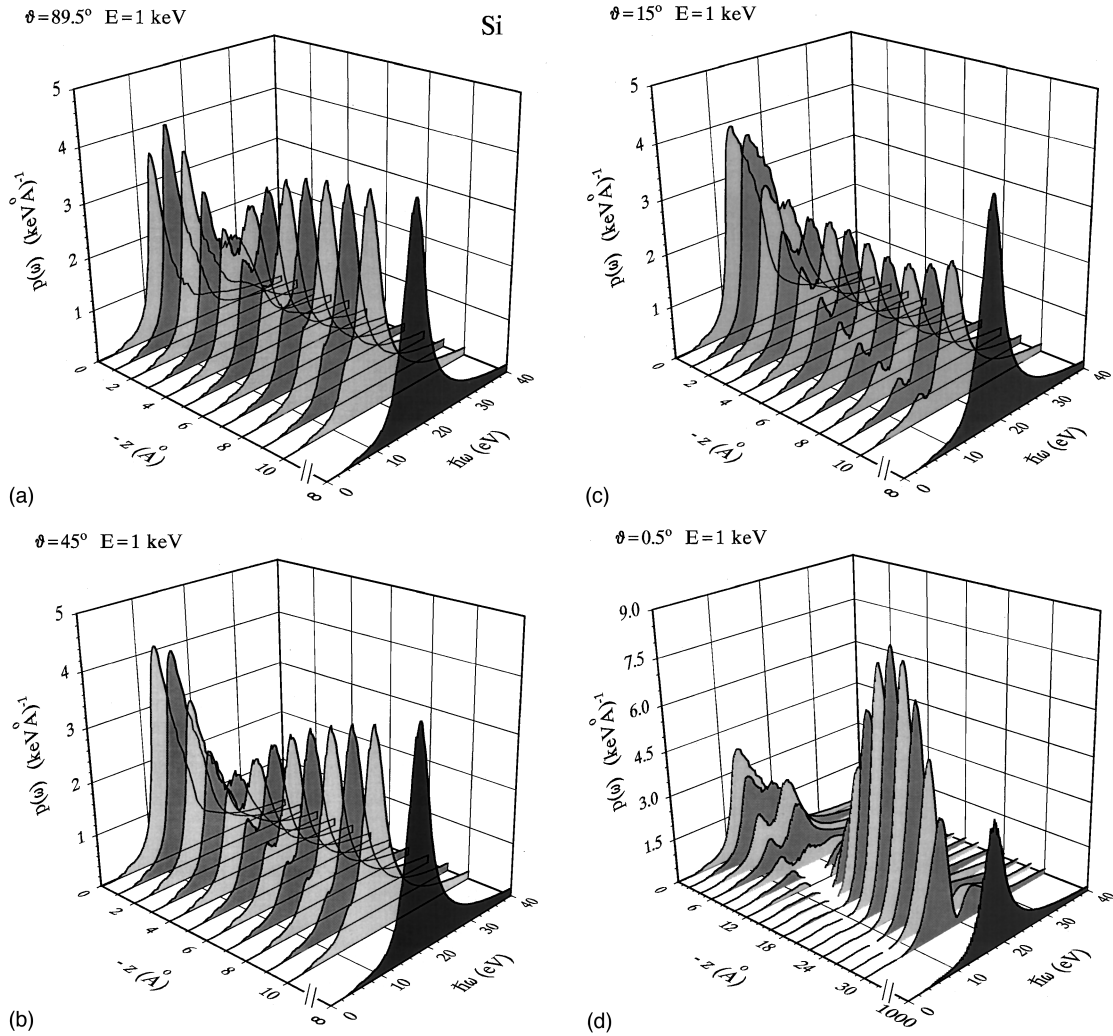
FIG. 7. Plots of the depth dependence of the total differential cross section at a constant kinetic energy $E=1$ keV for Si and for takeoff angles (a) 89.5°, (b) 45°, (c) 15°, and (d) 0.5°. Note that the scales in (d) are different from those in (a)–(c). The cross-section values at $z=-10^3$ Å in (d) are nearly the same as the bulk values shown by the curves at $z=-\infty$ in (a)–(c).

able excitations near the surface region are nearly at ~ 1 Å under the surface even for ϑ as small as 45°.

The z dependence modifies the measured spectra in an experiment through the factors of the experimental configuration. Changing the incident electron beam to the surface normal direction and increasing the primary beam energy, the interaction volume goes down into the deep interior of the target and bulk excitation dominates the inelastic scattering mechanism. Varying the detection angle to a glancing condition, only those signal electrons localized in the surface region can contribute to a spectrum and the surface excitation is a major effect in this case.

It should be noted that Eq. (25) tells us in theory that the image charge term vanishes for $z \rightarrow -\infty$ through a cosine factor oscillating both in z and ω. The surface charge term has similar oscillating behavior but with a different phase. Equation (B1) states that after angular integration the amplitude of the oscillatory factor strongly depends on the values of $v_\parallel$, i.e., the amplitude and direction of the velocity vector. This turns on the angular dependence. If the takeoff angle is very large the oscillation behavior in z can only be observed

for very small $-z$, as displayed in Fig. 7 and discussed above. For large $-z$ values, the phase of the oscillatory factor varies rapidly with ω as well as ω_p so that the energy integration of these factors over ω_p smears out to zero. The total differential cross section quickly approaches the value of bulk cross section with increasing depth.

However, in the case of near normal ejection, $\vartheta \sim 0$, the oscillation is clearly seen in Figs. 7(d) and 8(d). As can be seen from Eq. (B1), for $v_\parallel \rightarrow 0$, the second term tends to zero and the first term becomes a δ function that may be expressed as $\delta(\omega_p - (\omega^2/2v^2 + q_\parallel^2/2 - \omega))$. Hence, the integration over ω_p is performed mainly for a single-phase factor. The shape of $p^{b-s}(\omega)$ is simply the bulk energy-loss function modulated by the oscillating factor. For sufficiently large $-z$, the bulk term still dominates the total differential cross section because of the phase difference in $q_\parallel$. This oscillation comes from the dispersion of the dielectric function in the plasmon-pole approximation, as indicated by comparing Eq. (A4) with Eq. (A6). The modulated peak position in ω and peak intensity changes with z continuously, as shown by Fig. 8(d). An ejected electron from the surface carries little infor-
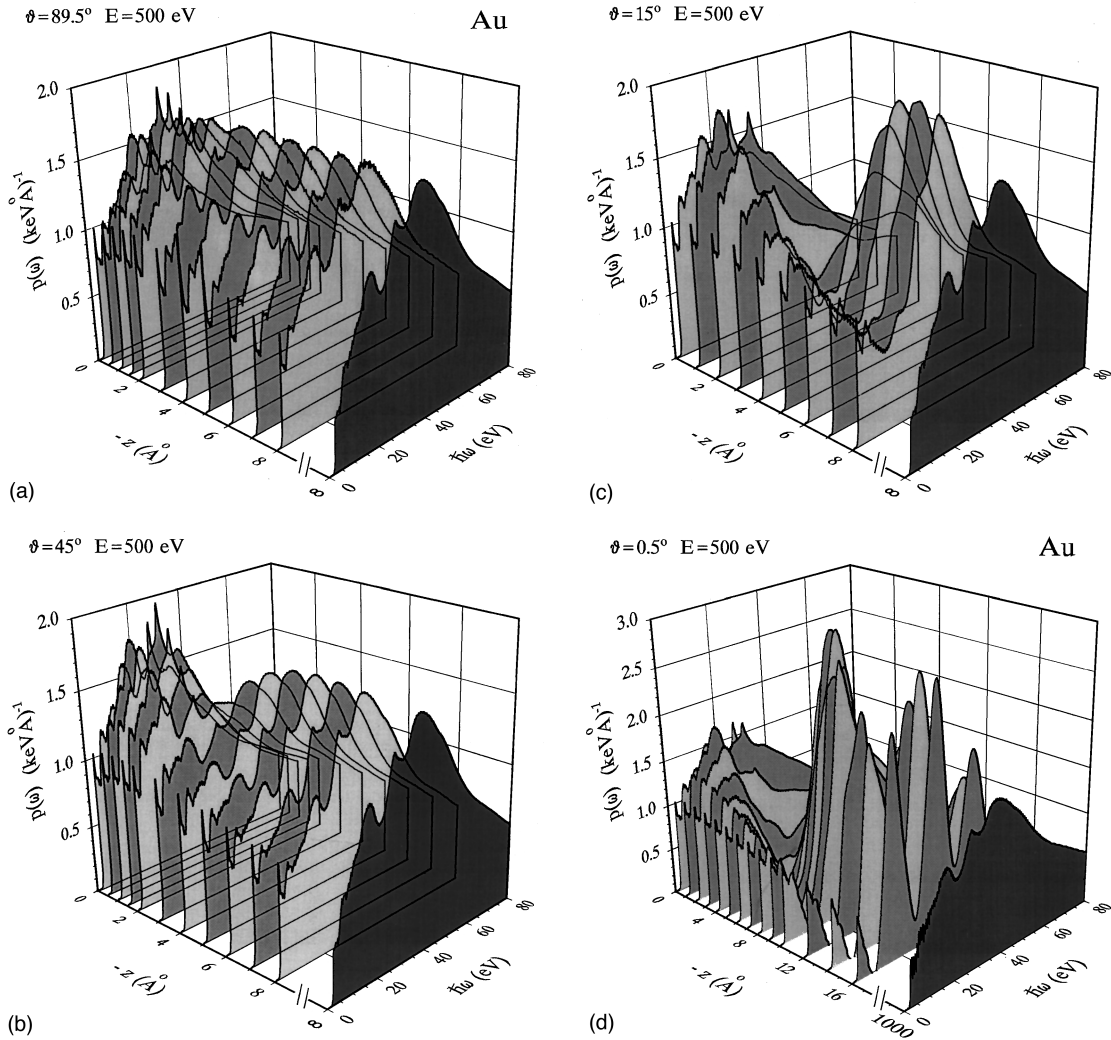
FIG. 8. Plots of the depth dependence of the total differential cross section at a constant kinetic energy $E=1$ keV for Au and for takeoff angles (a) 89.5°, (b) 45°, (c) 15°, and (d) 0.5°. Note that the scales in (d) are different from those in (a)–(c). The cross-section values at $z=-10^3$ Å in (d) are nearly the same as the bulk values shown by the curves at $z=-\infty$ in (a)–(c).

mation of such modulation. In addition, signal electrons frequently change their moving direction by elastic scattering during their travel to the surface. Hence, the energy-loss distribution for ejected electrons from a sample is qualitatively described by the surface energy-loss function for surface mode excitation and the bulk energy-loss function for bulk mode excitation.

A direct application of the present theory is for a Monte Carlo simulation of electron scattering processes near the surface region. It is obvious that the experimentally measured spectra include much information about electron elastic and inelastic scattering events, such as angular distribution and energy-loss distribution with energy dependence, depth dependence, and angular dependence. Some instrumental factors such as detector solid angles also complicate the analysis. To verify an electron scattering theory, it is essential to use the means of simulation and compare the results with experimental measurement. We have shown[56] that the bulk scattering cross section alone successfully describes the overall shape of backscattering spectrum for high-energy (about several keV) incident electrons into metals.

But the bulk model fails in experimental conditions that surface effect dominates the measured spectra, e.g., at lower primary energy and large incident and takeoff angles. Some Monte Carlo models[57,58] have been used to study electron-surface interaction. However, some information, such as the knowledge of the depth dependence particularly, has not been included in these models. Therefore, the present theory is more informative in this respect.

IV. CONCLUSION

We have presented a theoretical model for the calculation of electron inelastic scattering cross sections for a moving electron near the surface region at an arbitrary takeoff angle. By using a bulk plasmon-pole approximation, we have derived an expression of the imaginary part of the electron self-energy. The numerical values of the double differential cross section in energy loss and horizontal momentum transfer, and the differential cross section in energy loss with dependence on kinetic energy, takeoff angle, and depth, can be obtained by numerical integration. Input to the calculation

is simply the dielectric constants $\varepsilon(\omega)$. The theory provides detailed information of the electron energy-loss process near the surface region of a real metal, and, should find very useful applications to surface electron spectroscopy as well as to a Monte Carlo simulation of electron scattering processes in a metal.

Examples of calculations have been demonstrated for Si and Au. We have shown that for electrons located deep inside the metal, bulk mode excitation is the only inelastic scattering channel. In the surface region, the surface mode excitation is turned on. The relative importance of the surface effect depends on the energy and takeoff angle. For Au, the surface mode has also displayed a broadened distribution in frequency. The peak at 2.6 eV in an experimental energy-

loss spectrum should largely be attributed to the surface mode.

APPENDIX A

Assuming the dispersion relation given by Eq. (22), we have

$$\int_{-\infty}^{\infty} \frac{dq_\perp}{q^2(\omega^2-\omega_q^2+i\eta)} = \frac{\pi}{q_\parallel}\mathcal{P}\frac{1}{\omega^2-\omega_p^2} - \frac{\pi}{2\omega}\left[\frac{1}{(\omega+\omega_p)\sqrt{2(\omega+\omega_p)+q_\parallel^2}} + \mathcal{P}\frac{\theta(\omega_p-\omega+q_\parallel^2/2)}{(\omega-\omega_p)\sqrt{2(\omega_p-\omega)+q_\parallel^2}}\right.$$

$$\left. +i\frac{\theta(\omega-\omega_p-q_\parallel^2/2)}{(\omega-\omega_p)\sqrt{2(\omega-\omega_p)-q_\parallel^2}}\right]. \tag{A1}$$

Similarly, another integration term involved in Eq. (11) is obtained as

$$\frac{q_\parallel}{\pi}\int_{-\infty}^{\infty}e^{iq_\perp z}\frac{dq_\perp}{q^2\varepsilon(q,\omega)} = e^{q_\parallel z}\,\text{Re}\left\{\frac{1}{\varepsilon(\omega)}\right\} - \frac{1}{\pi\omega}\int_0^{\infty}d\omega_p\omega_p\,\text{Im}\left\{\frac{-1}{\varepsilon(\omega_p)}\right\}\left[\frac{1}{(\omega+\omega_p)\sqrt{2(\omega+\omega_p)/q_\parallel^2+1}}\,e^{\sqrt{2(\omega+\omega_p)+q_\parallel^2}\,z}\right.$$

$$+\mathcal{P}\frac{\theta(\omega_p-\omega+q_\parallel^2/2)}{(\omega-\omega_p)\sqrt{2(\omega_p-\omega)/q_\parallel^2+1}}\,e^{\sqrt{2(\omega_p-\omega)+q_\parallel^2}\,z}$$

$$\left. +i\frac{\theta(\omega-\omega_p-q_\parallel^2/2)}{(\omega-\omega_p)\sqrt{2(\omega-\omega_p)/q_\parallel^2-1}}\,e^{-i\sqrt{2(\omega-\omega_p)-q_\parallel^2}\,z}\right]. \tag{A2}$$

Now we need to solve the integration in Eqs. (10) and (11) involving the velocity vector:

$$F_n^{\pm} \equiv \int_{-\infty}^{\infty}\frac{dq_\perp}{q^2\varepsilon(q,\omega)}\frac{e^{\pm inq_\perp z}}{\omega-\mathbf{q}\cdot\mathbf{v}\pm i\eta} = \int_{-\infty}^{\infty}\frac{dq_\perp}{q^2}\frac{e^{\pm inq_\perp z}}{\omega-\mathbf{q}\cdot\mathbf{v}\pm i\eta} + \int_0^{\infty}d\omega_p H(\omega_p)$$

$$\times\left[\int_{-\infty}^{\infty}\frac{dq_\perp}{q^2}\frac{e^{\pm inq_\perp z}}{(\omega_q+\omega+i\eta)(\omega-\mathbf{q}\cdot\mathbf{v}\pm i\eta)} - \int_{-\infty}^{\infty}\frac{dq_\perp}{q^2}\frac{e^{\pm inq_\perp z}}{(\omega_q-\omega-i\eta)(\omega-\mathbf{q}\cdot\mathbf{v}\pm i\eta)}\right], \tag{A3}$$

whose result obviously depends on the sign of $v_\perp$. In the present case we are interested in electrons moving toward the surface from the interior of the bulk. Hence, for $z<0$, the integration contour must be closed in the lower-half plane of $q_\perp$ for F_n^+ and in the upper-half plane for F_n^-. Because $v_\perp>0$, the term $(\omega-\mathbf{q}\cdot\mathbf{v}\pm i\eta)$ in the denominator of the integrand is not a pole enclosed in the respective contour and would not contribute a residue.

The first integral term in Eq. (A3) has a simple pole due to q^2, therefore,

$$\int_{-\infty}^{\infty} \frac{dq_\perp}{q^2} \frac{e^{\pm inq_\perp z}}{\omega - \mathbf{q}\cdot\mathbf{v} \pm i\eta} = \frac{\pi}{q_\parallel} \frac{e^{nq_\parallel z}}{\omega - \mathbf{q}_\parallel\cdot\mathbf{v}_\parallel \pm iq_\parallel v_\perp}. \tag{A4}$$

The first integral in square brackets in Eq. (A3) contains an additional pole by the ω_q factor. The evaluation of the residues leads to

$$\int_{-\infty}^{\infty} \frac{dq_\perp}{q^2} \frac{e^{\pm inq_\perp z}}{(\omega_q + \omega + i\eta)(\omega - \mathbf{q}\cdot\mathbf{v} \pm i\eta)} = \frac{\pi}{\omega + \omega_p}\left[\frac{1}{q_\parallel}\frac{e^{nq_\parallel z}}{\omega - \mathbf{q}_\parallel\cdot\mathbf{v}_\parallel \pm iq_\parallel v_\perp} \right.$$

$$\left. - \frac{1}{\sqrt{2(\omega+\omega_p)+q_\parallel^2}} \frac{e^{n\sqrt{2(\omega+\omega_p)+q_\parallel^2}z}}{\omega - \mathbf{q}_\parallel\cdot\mathbf{v}_\parallel \pm i\sqrt{2(\omega+\omega_p)+q_\parallel^2}v_\perp} \right]. \tag{A5}$$

To evaluate the second integral in square brackets in Eq. (A3) we need to consider two cases: When $\omega \geq \omega_p + q_\parallel^2/2$, the ω_q factor contributes two poles at $q_\perp = \pm[\sqrt{2(\omega-\omega_p)-q_\parallel^2} + i\eta]$. For the case $\omega < \omega_p + q_\parallel^2/2$, two poles are at $q_\perp = \pm i\sqrt{2(\omega_p - \omega) + q_\parallel^2}$. Hence, we have

$$\int_{-\infty}^{\infty} \frac{dq_\perp}{q^2} \frac{e^{\pm inq_\perp z}}{(\omega_q - \omega - i\eta)(\omega - \mathbf{q}\cdot\mathbf{v}\pm i\eta)} = \mathcal{P}\frac{\pi}{\omega_p - \omega}\left[\frac{1}{q_\parallel}\frac{e^{nq_\parallel z}}{\omega - \mathbf{q}_\parallel\cdot\mathbf{v}_\parallel \pm iq_\parallel v_\perp} \right.$$

$$\left. - \frac{\theta(\omega_p - \omega + q_\parallel^2/2)}{\sqrt{2(\omega_p-\omega)+q_\parallel^2}} \frac{e^{n\sqrt{2(\omega_p-\omega)+q_\parallel^2}z}}{\omega - \mathbf{q}_\parallel\cdot\mathbf{v}_\parallel \pm i\sqrt{2(\omega_p-\omega)+q_\parallel^2}v_\perp} \right]$$

$$+ i\frac{\pi}{\omega-\omega_p} \frac{\theta(\omega - \omega_p - q_\parallel^2/2)}{\sqrt{2(\omega-\omega_p)-q_\parallel^2}} \frac{e^{-in\sqrt{2(\omega-\omega_p)-q_\parallel^2}z}}{\omega - \mathbf{q}_\parallel\cdot\mathbf{v}_\parallel \pm [\sqrt{2(\omega-\omega_p)-q_\parallel^2}v_\perp + i\eta]}. \tag{A6}$$

Substituting Eqs. (A4)–(A6) into Eq. (A3) gives

$$F_n^- - F_n^+ = \int_{-\infty}^{\infty} \frac{dq_\perp}{q^2 \varepsilon(q,\omega)} \left(\frac{e^{-inq_\perp z}}{\omega - \mathbf{q}\cdot\mathbf{v} - i\eta} - \frac{e^{inq_\perp z}}{\omega - \mathbf{q}\cdot\mathbf{v} + i\eta} \right)$$

$$= 2\pi i \frac{v_\perp e^{nq_\parallel z}}{(\omega - \mathbf{q}_\parallel\cdot\mathbf{v}_\parallel)^2 + (q_\parallel v_\perp)^2} \operatorname{Re}\left\{ \frac{1}{\varepsilon(\omega)} \right\} - 2\pi i\frac{1}{\pi\omega}\int_0^\infty d\omega_p \omega_p \operatorname{Im}\left\{ \frac{-1}{\varepsilon(\omega_p)} \right\}$$

$$\times \left\{ \frac{v_\perp e^{n\sqrt{2(\omega+\omega_p)+q_\parallel^2}z}}{(\omega+\omega_p)\{(\omega - \mathbf{q}_\parallel\cdot\mathbf{v}_\parallel)^2 + [2(\omega+\omega_p)+q_\parallel^2]v_\perp^2\}} + \mathcal{P}\frac{v_\perp \theta(\omega_p - \omega + q_\parallel^2/2)e^{n\sqrt{2(\omega_p-\omega)+q_\parallel^2}z}}{(\omega-\omega_p)\{(\omega - \mathbf{q}_\parallel\cdot\mathbf{v}_\parallel)^2 + [2(\omega_p-\omega)+q_\parallel^2]v_\perp^2\}} \right.$$

$$\left. + \frac{v_\perp \theta(\omega - \omega_p - q_\parallel^2/2)e^{-in\sqrt{2(\omega-\omega_p)-q_\parallel^2}z}}{(\omega-\omega_p)\{(\omega - \mathbf{q}_\parallel\cdot\mathbf{v}_\parallel)^2 - [2(\omega-\omega_p)-q_\parallel^2]v_\perp^2 - i\eta\}} \right\}. \tag{A7}$$

In Eqs. (10) and (11), a further integration over $\mathbf{q}_\parallel$ is applied. Due to an infinitesimal quantity the last term in the large bracket of the above equation can be split into a principle value, the real part, and a δ-function, the imaginary part. Then performing an angular integration over $\varphi = (\widehat{\mathbf{q}_\parallel, \mathbf{v}_\parallel})$ and deforming the integration contour into a unit circle, the integration of the principle value part equals zero because there is no pole inside the circle. Hence, the term only remains a δ-function part being

$$i\frac{\pi}{2} \frac{\theta(\omega - \omega_p - q_\parallel^2/2)}{(\omega-\omega_p)\sqrt{2(\omega-\omega_p)-q_\parallel^2}} e^{-in\sqrt{2(\omega-\omega_p)-q_\parallel^2}z}\left[\delta(\omega - \mathbf{q}_\parallel\cdot\mathbf{v}_\parallel - \sqrt{2(\omega-\omega_p)-q_\parallel^2}v_\perp) + \delta(\omega - \mathbf{q}_\parallel\cdot\mathbf{v}_\parallel + \sqrt{2(\omega-\omega_p)-q_\parallel^2}v_\perp) \right].$$

$$\tag{A8}$$

APPENDIX B

In Eq. (25), the integration over polar angles of $\mathbf{q}_\parallel$ may be calculated first to find a simple expression,

$$\int_0^{2\pi} d\varphi [\delta(\omega - q_\parallel v_\parallel \cos \varphi - a) + \delta(\omega - q_\parallel v_\parallel \cos \varphi + a)]$$

$$= 2 \left\{ \frac{\theta[q_\parallel v_\parallel - |\omega - a|]}{\sqrt{(q_\parallel v_\parallel)^2 - (\omega - a)^2}} + \frac{\theta[q_\parallel v_\parallel - (\omega + a)]}{\sqrt{(q_\parallel v_\parallel)^2 - (\omega + a)^2}} \right\}, \quad (B1)$$

where $a = \sqrt{2(\omega - \omega_p) - q_\parallel^2} v_\perp$, by using the relation

$$\delta[f(x)] = \sum_i \delta(x - x_i)/|f'(x_i)|, \quad (B2)$$

where $f(x_i) = 0$. The integration over photon energy ω_p can then be performed numerically afterwards. However, this procedure needs longer computer time since a large number of sampling points in ω_p are necessary. Instead, the integration over ω_p may be done analytically by preceding the numerical integration over φ with a smaller number of data grids but without losing accuracy. Hence, we used

$$\int_0^\infty d\omega_p f(\omega_p) a^{-1} [\delta(\omega - \mathbf{q}_\parallel \cdot \mathbf{v}_\parallel - a) + \delta(\omega - \mathbf{q}_\parallel \cdot \mathbf{v}_\parallel + a)]$$

$$= 2 f(\bar{\omega}_p), \quad (B3)$$

where

$$\bar{\omega}_p = \omega - \tfrac{1}{2}[q_\parallel^2 + (\omega - \mathbf{q}_\parallel \cdot \mathbf{v}_\parallel)^2 / v_\perp^2]. \quad (B4)$$

To calculate $\mathrm{Im}\,\Sigma_{\mathrm{in}}^s(z)$ we have to derive the expression of angular integration for the other terms in Eq. (A7). Denoting

$$I = \int_0^{2\pi} \frac{d\varphi}{(\omega - q_\parallel v_\parallel \cos \varphi)^2 + b^2}, \quad (B5)$$

where b equals $\sqrt{2(\omega + \omega_p) + q_\parallel^2} v_\perp$ or $\sqrt{2(\omega_p - \omega) + q_\parallel^2} v_\perp$, the integration value is found from residues of two poles in the unit circle of $e^{i\varphi}$, as

$$I = \frac{\pi i}{b} \frac{1}{q_\parallel v_\parallel} \left(\frac{1}{\sqrt{(\alpha + i\beta)^2 - 1}} - \frac{1}{\sqrt{(\alpha - i\beta)^2 - 1}} \right), \quad (B6)$$

where $\alpha = \omega/(q_\parallel v_\parallel)$ and $\beta = b/(q_\parallel v_\parallel)$. In the above equation the principle value of the roots should be taken. This may be easily seen by considering the case of parallel electron movement to the surface. In the limit $b \to 0$ the integrand of bI becomes $\pi \delta(\omega - q_\parallel v_\parallel \cos \varphi)$ and, hence, can be integrated and compared with Eq. (B6).

[1] S. Tougaard, Surf. Interface Anal. **11**, 453 (1988).
[2] F. Yubero and S. Tougaard, Phys. Rev. B **46**, 2486 (1992).
[3] H. Yoshikawa, R. Shimizu, and Z.-J. Ding, Surf. Sci. **261**, 403 (1992).
[4] D. M. Newns, Phys. Rev. B **8**, 3304 (1970).
[5] J. Heinrichs, Phys. Rev. B **8**, 1346 (1973).
[6] D. Gumhalter and D. M. Newns, Surf. Sci. **50**, 465 (1975).
[7] D. Chan and P. Richmond, J. Phys. C **9**, 163 (1976).
[8] J. P. Muscat, Solid State Commun. **18**, 1089 (1976).
[9] D. L. Mills, Phys. Rev. B **15**, 763 (1977).
[10] T. L. Ferrell, P. M. Echenique, and R. H. Ritchie, Solid State Commun. **32**, 419 (1979).
[11] R. Nunez, P. M. Echenique, and R. H. Ritchie, J. Phys. C **13**, 4229 (1980).
[12] P. M. Echenique, R. H. Ritchie, N. Barberan, and J. Inkson, Phys. Rev. B **23**, 6486 (1981).
[13] A. G. Eguiluz, Phys. Rev. B **23**, 1542 (1981).
[14] P. M. Echenique, Philos. Mag. B **52**, L9 (1985).
[15] A. Gras-Marti, P. M. Echenique, and R. H. Ritchie, Surf. Sci. **173**, 310 (1986).
[16] P. M. Echenique, J. Bausells, and A. Rivacoba, Phys. Rev. B **35**, 1521 (1987).
[17] N. Zabala and P. M. Echenique, Ultramicroscopy **32**, 327 (1990).
[18] J. L. Gervasoni and N. R. Arista, Surf. Sci. **260**, 329 (1992).
[19] R. H. Ritchie and A. Howie, Philos. Mag. **36**, 463 (1977).
[20] D. R. Penn, Phys. Rev. B **35**, 482 (1987).
[21] L. Hedin and S. Lundqvist, in *Solid State Physics*, edited by S. Seitz, D. Turnbull, and H. Ehrenreich (Academic, New York, 1969), Vol. 23, pp. 1–181.
[22] A. W. Overhauser, Phys. Rev. B **3**, 1888 (1971).
[23] J. C. Ashley, J. Electron Spectrosc. Relat. Phenom. **46**, 199 (1988).
[24] S. Tanuma, C. J. Powell, and D. R. Penn, Surf. Interface. Anal. **11**, 577 (1988).
[25] Z.-J. Ding and R. Shimizu, Surf. Sci. **222**, 313 (1989).
[26] J. C. Ashley, J. Appl. Phys. **69**, 674 (1991).
[27] J. M. Fernandez-Verea, R. Mayol, F. Salvat, and D. Liljequist, J. Phys. C **4**, 2879 (1992).
[28] P. M. Echenique and J. B. Pendry, Prog. Surf. Sci. **32**, 111 (1990).
[29] F. Flores and F. Garcia-Moliner, J. Phys. C **12**, 907 (1979). The sign of the first term in Eq. (6.1) should be minus.
[30] R. H. Ritchie and A. L. Marusak, Surf. Sci. **4**, 234 (1966).
[31] F. Garcia-Moliner and F. Flores, *Introduction to the Theory of Solid Surfaces* (Cambridge University, Cambridge, 1979).
[32] Z.-J. Ding (unpublished).
[33] P. M. Echnique and R. H. Ritchie, Phys. Rev. B **20**, 2567 (1979).
[34] C. J. Tung, J. C. Ashley, and R. H. Ritchie, Surf. Sci. **81**, 427 (1979).
[35] D. W. Johnson, J. Phys. A **8**, 490 (1975).
[36] K.-D. Tsuei, E. W. Plummer, and P. J. Feibelman, Phys. Rev. Lett. **63**, 2256 (1989).
[37] P. T. Sprunger, G. M. Watson, and E. W. Plummer, Surf. Sci. **269/270**, 551 (1992).
[38] P. J. Feibelman, Prog. Surf. Sci. **12**, 287 (1982).
[39] A. Liebsh, Phys. Rev. B **36**, 7378 (1987).
[40] D. F. Edwards, in *Handbook of Optical Constants of Solids*, ed-

ited by E. D. Palik (Academic, Orlando, 1985); D. W. Lynch and W. R. Hunter, *ibid*.

[41] G. D. Mahan, *Many Particle Physics* (Plenum, New York, 1981).

[42] B. Gumhalter, J. Phys. (Paris) **38**, 1117 (1975).

[43] B. Gumhalter and D. M. Newns, Phys. Lett. **53A**, 137 (1975).

[44] D. Lovric and B. Gumhalter, Phys. Rev. B **38**, 10 323 (1988).

[45] M. Sunjic and A. A. Lucas, Phys. Rev. B **3**, 719 (1971).

[46] A. A. Lucas, in *Collective Excitations in Solids*, edited by B. D. Bartolo (Plenum, New York, 1983).

[47] O. Sueoka and F. Fujimoto, J. Phys. Soc. Jpn. **20**, 569 (1965).

[48] N. E. Christensen and B. O. Seraphin, Phys. Rev. B **4**, 3321 (1971).

[49] M. Creuzburg, Z. Phys. **196**, 433 (1966).

[50] J. Thirlwell, Proc. R. Soc. London **91**, 552 (1967).

[51] J. C. Ingram, K. W. Nebesny, and J. E. Pemberton, Appl. Surf. Sci. **44**, 293 (1990).

[52] C. J. Tung, Y. F. Chen, C. M. Kwei, and T. L. Chou, Phys. Rev. B **49**, 16 684 (1994).

[53] H. Yoshikawa, Y. Irokawa, and R. Shimizu, J. Vac. Sci. Technol. A **13**, 1984 (1995).

[54] F. Yubero, J. M. Sanz, B. Ramskov, and S. Tougaard, Phys. Rev. B **53**, 9719 (1996).

[55] T. Nagatomi, Z.-J. Ding, and R. Shimizu, Surf. Sci. **359**, 163 (1995).

[56] Z.-J. Ding, T. Nagatomi, R. Shimizu, and K. Goto, Surf. Sci. **336**, 397 (1995).

[57] P. Dubot, D. Jousset, V. Pinet, F. Pellerin, and J. P. Langeron, Surf. Interface Anal. **12**, 99 (1988).

[58] Y. F. Chen, J. Vac. Sci. Technol. A **13**, 2665 (1995).